Available online at www.sciencedirect.com
ScienceDirect
Journal of Catalysis 247 (2007) 43–50
JOURNAL OF CATALYSIS
www.elsevier.com/locate/jcat

Esterification and transesterification on tungstated zirconia: Effect of calcination temperature

Dora E. López, Kaewta Suwannakarn, David A. Bruce, James G. Goodwin Jr. *

Department of Chemical and Biomolecular Engineering, Clemson University, Clemson, SC 29634, USA

Received 9 October 2006; revised 8 January 2007; accepted 9 January 2007

Available online 12 February 2007

Abstract

As part of ongoing efforts to investigate heterogeneous catalysts for biodiesel synthesis, the catalytic activity of the strong solid acid tungstated zirconia (WZ) was studied for the esterification of acetic acid (in both the gas and liquid phase) and the transesterification of triacetin (a synthetic triglyceride in the liquid phase) with methanol. Acetic acid and triacetin were used as model compounds for free fatty acids (FFAs) and triglycerides, respectively. Complex mixtures of FFAs and triglycerides are typical biodiesel precursors found in unrefined vegetable oils, animal fats, and waste greases. The effect of calcination temperature (400–900 °C) on the catalytic properties of WZ was investigated with the goal of determining the optimum pretreatment temperature and increasing the understanding of the nature of the active sites for esterification and transesterification. Catalyst characterization by powder X-ray diffraction, Raman spectroscopy, TGA, elemental analysis, and total BET surface area allowed us to correlate the changes in catalyst physicochemical properties with calcination temperature. Ion-exchange/titration and NH_3-TPD were used to characterize the number and strength of the acid sites. Esterification and transesterification rates (on a catalyst weight basis) increased with increasing surface WO_x densities between 1.9 and 6.6 W-atoms nm^{-2} and then decreased for densities above 6.6 W-atoms nm^{-2}. The growth of WO_3 crystalline species resulted in lower esterification and transesterification rates, consistent with a decrease in the number of active sites. For the catalyst that exhibited the optimum catalytic activity (calcined at 800 °C), selective poisoning of the potential catalytic centers revealed that Brønsted sites play the major role in carrying out these reactions.

Keywords: Acetic acid; Triacetin; Esterification; Transesterification; Tungstated zirconia; WZ; Calcination effect; Selective poisoning; Brønsted versus Lewis acidity; Sites

1. Introduction

Environmental and economic considerations have made the production of renewable resource fuels highly advantageous. Biodiesel has received particular attention because it can be prepared from a variety of vegetable oils and animal fats and is readily used in existing diesel engines. Biodiesel production costs could be further improved if lower cost feedstocks, such as used cooking oils and animal fats, could be easily converted. These feedstocks often contain significant quantities of free fatty acids (FFAs) and water, which make them unsuitable for existing homogeneous alkaline-catalyzed processes. Neutralization of FFAs can be carried out by the addition of excess alkali, but this leads to the formation of soaps and to post-reaction separation problems. Thus, a preferred pretreatment process for used cooking oils is an esterification process that commonly uses a strong liquid acid catalyst, such as sulfuric acid [1–5]. However, the use of this strong acid mandates the use of costly corrosion-resistant materials and neutralization of the reaction mixture after esterification before the subsequent homogeneous base-catalyzed transesterification.

The use of solid acid catalysts offers many advantages over existing homogeneous catalysts used in biodiesel synthesis [6]. For example, solid acid catalysts have the ability to simultaneously catalyze transesterification and esterification reactions. Among strong solid acid catalysts, sulfated zirconia (SZ) and Nafion resin catalysts have been shown to catalyze biodiesel forming reactions as efficiently as sulfuric acid on a site activity basis [7,8]. Nevertheless, SZ is known to suffer significant

* Corresponding author. Fax: +1 864 656 0784.
E-mail address: james.goodwin@ces.clemson.edu (J.G. Goodwin Jr.).

0021-9517/$ – see front matter
doi:10.1016/j.jcat.2007.01.003

deactivation during liquid-phase transesterification [7,9], possibly due to sulfur leaching at even mild temperatures (60 °C). Nafion resins (e.g., NafionSAC-13 and NafionNR50), on the other hand, are effective in esterification and transesterification reactions [7,8,10–12] and tend to maintain higher catalytic activities, especially when the water byproduct is stripped off during reaction [12]. However, to preserve resin stability, the temperature of operation must be kept below 280 °C [8], and there is evidence that larger reactant molecules lead to greater deactivation, perhaps due to entanglement with the catalyst polymeric chains [11].

Supported tungsten oxide catalysts have recently received much attention because of their acid properties and their ability to catalyze both esterification and transesterification reactions, which play major roles in biodiesel production [7,13–15]. Furuta et al. [13] reported that soybean oil can be efficiently converted to methyl esters at a reaction temperature of 250 °C using tungstated zirconia alumina (WZA) calcined at 800 °C. The addition of Al_2O_3 further stabilizes the tetragonal phase of the ZrO_2 support and also prevents the growth of WO_3 particles [16]. WZA is also suitable for the esterification of *n*-octanoic acid, showing promise for application in biodiesel synthesis from lower-quality feedstocks. Another study that investigated the esterification of palmitic acid with methanol on WZ found correlations among the conversion of palmitic acid, the acidity of WZ (as measured by NH_3-TPD), and the percentage of tetragonal phase of the ZrO_2 support [14]. More recently, we have reported, based on turnover frequency (TOF) results, that WZ has a site activity comparable to H_2SO_4 for catalyzing biodiesel-forming transesterification reactions [7]. Another advantage of WZ is that catalyst deactivation appears to be not rapid for transesterification of triglycerides with methanol [7,13].

Earlier studies have used this strong acid catalyst for a variety of reactions, including alkane isomerization [17–21] and alcohol dehydration [22,23]. More fundamental studies of WZ have also examined how the nature of the active sites influences the observed catalytic activity of the material [24–35]. Hino and Arata [17,18] first reported the formation of so-called "superacid" sites ($H_0 = -14.52$) on WZ (13 wt% W) for isomerization of butane and pentane, as well as Friedel–Craft acylations as a function of preparation conditions and calcination temperatures. These authors found that heating a combination of tungsten species and zirconium oxide to temperatures that would create a tetragonal zirconia phase led to the formation of catalysts with higher activity. Since then, many investigations have attempted to characterize the active sites formed on WZ catalysts [24–35]. Iglesia and coworkers have extensively studied the structural changes of WZ with calcination and tungsten loading [20,22,23,31,33,36]. These authors showed that turnover rates (for xylene isomerization and alcohol dehydration) were solely a function of the tungsten surface density, which changes with tungsten loading and calcination temperature. Despite the great amount of literature dealing with WZ surface catalytic properties, agreement on what constitutes the most active sites has not yet been reached. However, it has been observed that the formation of surface polymeric tungsten species correlates well with increases in WZ catalyst activity [31].

The transesterification of triglycerides using acid catalysts has been little studied. A major objective of the present study was to increase the understanding of the catalytic activity of strong solid acids (WZ) for biodiesel-forming type reactions. Esterification of acetic acid (gas and liquid phase) and transesterification of triacetin (liquid phase) with methanol were used as probe reactions. Triacetin is a synthetic triglyceride-like molecule that has the shortest possible alkyl chain length (a single $–CH_3$ moiety on each branch). Of particular interest was the effect of calcination temperature on WZ catalytic activity for the transesterification of triglycerides, because, to the best of our knowledge, no previous publication has addressed this issue.

2. Experimental

2.1. Materials

Triacetin (99.5 wt%), methanol (99.9 wt%), acetic acid (99.7 wt%), methyl acetate (99 wt%), an acetin mixture (45 wt% diacetin, 26 wt% monoacetin, 25 wt% triacetin, and 4 wt% glycerol), pyridine (99.9%), and di-*tert*-butyl-pyridine (97%) were purchased from Sigma–Aldrich and used as received. For GC analysis, ethanol (99.5 wt%; Acros Organics) was used as a solvent and toluene (99.8 wt%; Fisher Scientific) was used as the internal standard. Amorphous tungstated zirconia hydroxide precursor, XZO1251 (16 wt% WO_3), was provided by Magnesium Electron, Inc. (MEI, Manchester, UK). To activate the catalyst, WZ precursor samples were dehydrated at 120 °C for 1 h and then pretreated for 3 h under an air (zero grade) atmosphere in a furnace at calcination temperatures between 400 and 900 °C.

2.2. Catalyst characterization

Elemental analysis for tungsten was performed using inductively coupled plasma emission spectroscopy (Galbraith Laboratory, Knoxville, TN). Catalyst samples were calcined at 700, 800, or 900 °C before shipping to the external laboratory for elemental analysis. Catalyst total surface area (S_{BET}) was determined using a multipoint BET method. Before S_{BET} analysis, the catalyst samples were degassed at 200 °C and 10^{-3} Torr for 3 h. Adsorption measurements were carried out using UHP N_2 at –196 °C in a Micromeritics ASAP 2020 device. Catalyst thermal stability and degradation behavior were determined by thermogravimetric analysis using a Perkin–Elmer Pyris 1 TGA. Sample weight changes were recorded as an amorphous WZ precursor sample (8 mg) was heated at a rate of 20 °C/min from room temperature to 1000 °C under an atmosphere of air (zero grade), similar to the catalyst calcination conditions. NH_3-TPD was used to determine the acid site concentration and strength distribution of the WZ samples, as described previously [7]. The number of acid sites was also estimated by using a method involving an aqueous ion-exchange step of the catalyst H^+

ions with Na^+ ions, followed by titration of the resulting solution [8]. Monochromatic powder X-ray diffractograms were recorded in the 20°–70° 2θ range using an XDS 2000 instrument (Scintag Inc.). The diffractometer used Cu$K\alpha$ radiation with a wavelength of $\lambda = 1.54$ Å. The Raman spectra of the calcined WZ samples were obtained at room temperature in an air atmosphere. Raman measurements were carried out in a Renishaw Raman microspectrometer 100 equipped with a 26-mW near-infrared diode laser source ($\lambda = 785$ nm). The spectral range 0–3000 cm^{-1} was studied. The instrument was calibrated using a standard silica reference (520 cm^{-1}). GRAMS/32 software (Galactic Inc., Salem, NH) was used to analyze all spectra.

2.3. Reaction studies

2.3.1. Gas-phase esterification

Gas-phase esterification reactions were carried out in a flow differential stainless steel reactor (ID = 0.7 cm) at 120 °C, operated close to atmospheric pressure. Before the reaction, the catalyst was mixed with an inert solid (0.02 g WZ/0.28 g α-Al_2O_3) and pretreated in situ at 315 °C under a moisture-free air flow for 2 h. The reaction system was then cooled to the desired reaction temperature (120 °C) in flowing helium, and a mixed gas stream (120 cc/min) of acetic acid (HAc) and methanol vapor in helium from gas saturators was introduced into the reactor (concentration of HAc and methanol of 0.40 mmol/L). An equimolar ratio of 1:1 (HAc: methanol) was used, because preliminary results showed that methanol exhibited a negative reaction order under these experimental conditions. The concentrations of reactants at the reactor entrance and in the effluent stream were analyzed using a Varian CP-3380 GC equipped with an FID detector. A Varian CPWAX 52CB fused silica capillary column (60 m × 0.53 mm × 1 μm) was used for analyte separation. The injector and detector temperatures were set to 250 and 280 °C, respectively. For analyte separation, the GC oven temperature was held at 40 °C for 4 min; ramped at a rate of 5 °C/min to 50 °C, where it was held constant for 1 min; and finally ramped at 25 °C/min to 180 °C and held constant for 3.8 min. Initial reaction rates were determined at 5 min time on stream (TOS).

2.3.2. Liquid-phase esterification and transesterification

Initial liquid-phase reaction rates were investigated using an isothermal, well-mixed batch (1790 rpm) Parr reactor (model 4590). For transesterification, the reagent solution was poured into a 100-ml stainless steel reactor vessel. Then the reactants were heated to the desired temperature, and the solid catalyst (1 g ≡ 2 wt%) was added shortly after the reactor temperature reached the desired value. An analogous procedure was used for liquid-phase esterification reactions; although, to prevent the accumulation of water during reaction startup (due to autocatalysis) [37], acetic acid and 1 g (2 wt%) of catalyst were heated to 60 °C before methanol was added to the mixture. For both esterification and transesterification experiments, 49 g of the reagent solutions were used, and the reaction mixtures contained 100% excess of methanol (2× stoichiometry) as is typical for biodiesel synthesis (to shift equilibrium to the desired ester products). Sample aliquots (0.1 ml) were withdrawn periodically from the reactor, quenched to room temperature, and centrifuged in order to separate out the solid catalyst and prevent further reaction. Reaction sample concentrations were determined using an HP 6890 GC equipped with an FID as described previously [8]. Reactions were run for as long as 2 h, with initial rates determined from the concentration of diacetins and methyl acetate profiles (limiting reactant conversion <5%).

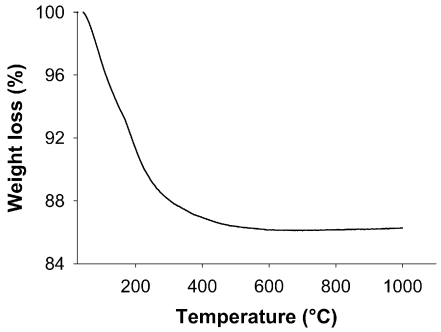

Fig. 1. Thermogravimetric analysis of uncalcined WZ precursor under an air atmosphere.

3. Results and discussion

3.1. Effect of calcination on WZ characteristics

The color of the catalyst changed from white to light yellow at high calcination temperatures (⩾800 °C), which is a qualitative indication of the formation of crystalline WO_3 particles [31]. Thermogravimetric analysis of the uncalcined WZ precursor in air showed a weight loss of about 14% at 500 °C (Fig. 1). This initial weight loss results from a loss of physisorbed and structural water. No further weight loss occurred from 500 to 1000 °C, indicating that no W is lost from the surface at higher calcination temperatures. Elemental analysis revealed that WZ samples calcined at 700, 800, and 900 °C had tungsten loadings of 13.4, 13.3, and 14.0 wt% W, respectively. These values are within expected experimental error with an average of 13.6 ± 0.4 wt% W.

The evolution of properties, such as surface area and pore volume, with respect to tungsten loading has been investigated previously [30]. Surface area decreased with calcination temperature (Table 1) as a result of loss of surface area of the ZrO_2 structure. For instance, after calcination at 900 °C, the surface area was only about 20% (58 m^2/g) of that of the dehydrated precursor (325 m^2/g). This loss of surface area is significantly inhibited by the presence of WO_x species [20,24,36]. Our results are in good agreement with previously reported BET measurements for WZ [24,35].

The effect of calcination temperature on the stability of the tetragonal phase of ZrO_2 was obtained using powder XRD of the calcined samples (Fig. 2). The catalyst calcined at 400 °C presented broad peaks (at 20°–40° and 40°–70° 2θ), indicating the presence of a somewhat X-ray–amorphous structure and possibly the existence of very small crystallites of tetragonal

Table 1
Surface area, theoretical W surface density, surface acidity, and XRD phases for WZ samples calcined at different temperatures

Calcination T (°C)	BET surface area (m^2/g)[a]	W surface density (W-atoms nm^{-2})	Surface acidity		XRD phases
			NH_3-TPD (μmol NH_3/g)[c]	Exchange/titration (μmol/g)[c]	
100	324	–	–	–	–
400	235	1.9	–	51	Somewhat amorphous
500	174	2.6	–	–	t-ZrO_2
600	114	3.9	74	100	t-ZrO_2
650	97	4.6	–	107	t-ZrO_2
700	86	5.2	54	137	t-ZrO_2
750	72[b]	6.2	–	–	t-ZrO_2
800	68	6.6	44	161	t-ZrO_2, WO_3
850	59[b]	7.5	–	90	t-ZrO_2, m-ZrO_2, WO_3
900	58	7.7	18	72	t-ZrO_2, m-ZrO_2, WO_3

[a] Experimental error ±9%.
[b] Estimated surface area (from the calcination temperature vs surface area correlation).
[c] Experimental error ±8%.

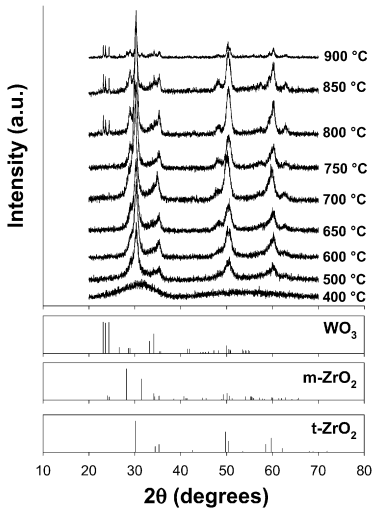

Fig. 2. Powder X-ray diffraction patterns for WZ calcined at different temperatures.

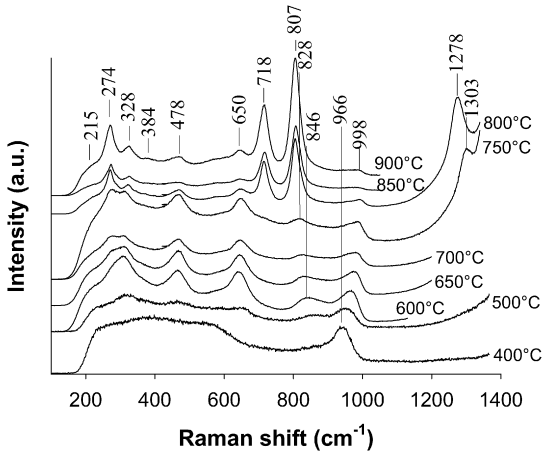

Fig. 3. Raman spectra of WZ calcined at different temperatures.

zirconia. At moderate calcination temperatures (500–800 °C), the catalyst contained primarily the tetragonal phase of zirconia, t-ZrO_2 (2θ diffraction peaks at 30.17°, 35.31°, and 49.79°). Further increases in the calcination temperature above 750 °C led to the formation of detectable bulk WO_3-like species with characteristic 2θ diffraction peaks at 23.12°, 23.59°, and 24.38°, which have been reported to appear when the W saturation coverage is exceeded [20]. Above a calcination temperature of 850 °C, the ZrO_2 support was largely tetragonal; however, the presence of the monoclinic phase of ZrO_2 ($2\theta = 28.17°$ and 31.47°) was also detected. The expected phase transition from tetragonal to monoclinic zirconia (m-ZrO_2) with increasing calcination temperature was most likely inhibited by the W surface density that helped to stabilize the tetragonal phase of ZrO_2 [28].

Using the values of surface area (at each calcination temperature) and the average W loading, it is possible to estimate nominal W surface densities [28,29] (Table 1). As a result of the loss in total surface area with increasing calcination temperature, the W oxide surface species undergo a transformation from monomeric to polymeric species [31]. For the WZ used in this study, surface saturation coverage (as defined by the formation of crystalline WO_3 as determined by powder XRD [23,28]) was achieved at densities of ∼6 W-atoms nm^{-2}, consistent with previous findings using similar materials. However, this value does not seem to be an absolute and may well depend on the catalyst preparation conditions. For instance, Barton et al. [31] found the coexistence of polytungstate and WO_3 species at surface densities >8 W-atoms nm^{-2}.

Raman spectroscopy was used to identify molecular level structural changes in the tungsten oxide overlayer and zirconium oxide support on calcination. Fig. 3 gives the Raman spectra results for the calcined WZ samples. The assignment of Raman bands was made by comparison with reference standards. Kilo et al. previously summarized the Raman frequencies corresponding to the crystalline structures of the zirconia support [38]. Using this information, the bands at 310–330, 470–475, and 647–655 cm^{-1} were assigned to the tetragonal phase of ZrO_2 and were found to be stronger for samples calcined within the 600–800 °C range. Only the sample calcined at 900 °C exhibited a weak band at ∼384 cm^{-1}, which is distinctive of m-ZrO_2. These observations are consistent with those obtained from powder XRD experiments.

Table 2
Raman bands assignment for tungsten oxide

Species	Raman shift (cm^{-1})	Ref.
WO_x	824, 1021	[19]
Terminal W=O	1019	[36]
	990–1020	[40]
	1001–1004	[50]
WO_3	275d, 720b, 808s	[31]
	274, 715, 807	[51]
	721, 810	[32]
	720, 807	[24]
	804s	[50]

Modes: (s) W–O stretching, (b) W–O bending, and (d) W–O–W deformation [31].

Table 2 provides a summary of the Raman bands assignment for the tungsten oxide overlayer species. The symmetric stretching bands of the terminal W=O, characteristic of tungsten species with various degrees of polymerization, progressively shifted from 846 cm^{-1} (600 °C) and 966 cm^{-1} (400 °C) to 828 cm^{-1} (750 °C) and 994 cm^{-1} (900 °C), respectively. Kuba et al. [39] showed that the shifting Raman band in the region of 952–976 cm^{-1} is detectable only when water is adsorbed on the catalyst surface, such as occurs here because the measurement was not made in a controlled atmosphere. The up-shift in the 990–1020 cm^{-1} region has been associated with the transition from mono- to poly-tungsten species with increasing W density [40]. The position of the Raman bands for crystalline WO_3 appeared only for samples calcined at $\geqslant$800 °C (bands at 273–275, 717–720, and 807–808 cm^{-1}), in agreement with powder XRD results. Thus, the formation of crystalline WO_3 was detectable at W surface densities above 6.6 W-atoms nm^{-2}. At such high W surface densities, the assignment of Raman bands becomes more complex because the bands for WO_3 crystalline structures tend to dominate the spectra and limit the detection of other WO_x species (band at 824 cm^{-1}) [19]. In addition, Raman bands in the frequency range of 1303 and 1278 cm^{-1} were detected only for samples calcined at 750 and 800 °C, respectively. No previous assignment of these bands was found, because previous analyses were typically reported only for the 0–1100 cm^{-1} range.

NH_3-TPD was used to compare the acidic characteristics of the catalysts calcined at 600, 700, 800, and 900 °C. NH_3 is a strong non-site-specific base ($pK_b \sim 5$) that under our experimental conditions titrates both surface Brønsted and Lewis acid sites. The TPD profiles revealed the coexistence of a broad distribution of acid site strengths (data not shown). It was also found that total acid site concentration decreased with calcination temperature (Table 1), which appeared to correlate with the loss of surface area. In contrast to NH_3-TPD estimations, the number of acid sites determined by the ion-exchange/titration method passed through a maximum for WZ calcined at 800 °C (where the W surface concentration was 6.6 W-atoms nm^{-2}). A study by Naito et al. [29], using NH_3-TPD with water vapor treatment for characterization of WZ acid sites, found a maximum in the concentration of acid sites at a W surface concentration of ca. 6.4 W-atoms nm^{-2} [29], in good agreement with our results obtained using the aqueous ion-exchange/titration method.

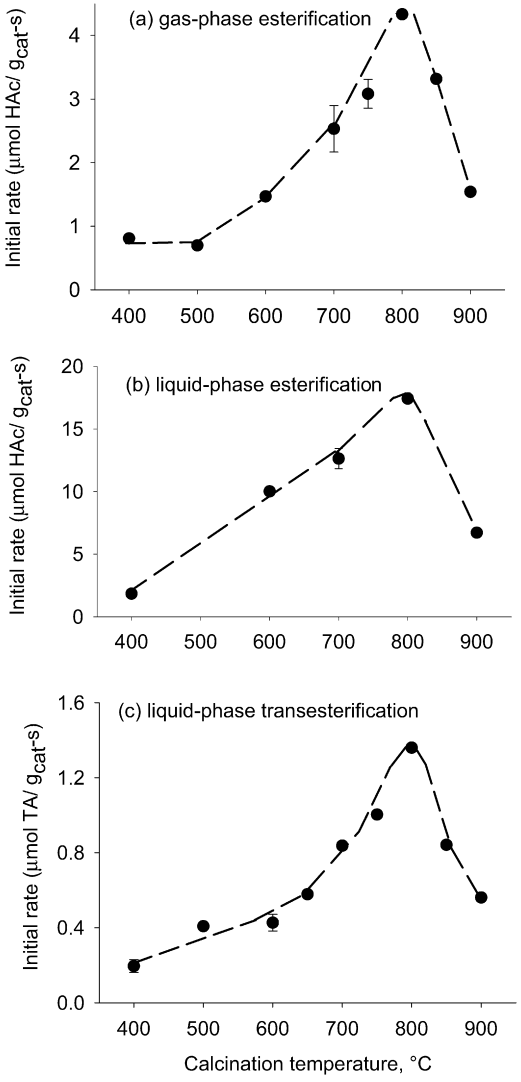

Fig. 4. Influence of calcination temperature on the activity of WZ for (a) gas-phase acetic acid esterification ($T_{rxn} = 120$ °C), (b) liquid-phase acetic acid esterification ($T_{rxn} = 60$ °C), and (c) liquid-phase triacetin transesterification ($T_{rxn} = 60$ °C).

3.2. *Effect of calcination temperature on esterification and transesterification*

Fig. 4 summarizes WZ initial activity results (conversion <5%) as a function of calcination temperature for acetic acid esterification (120 °C, gas phase; 60 °C, liquid phase) and triacetin transesterification (60 °C, liquid phase):

$$\text{acetic acid} + \text{methanol} \xleftrightarrow{\text{WZ}} \text{methyl acetate} + \text{water} \quad (1)$$

and

$$\text{triacetin} + \text{methanol} \xleftrightarrow{\text{WZ}} \text{methyl acetate} + \text{diacetin} \quad \text{(first step in the series)}. \quad (2)$$

For liquid-phase acetic acid esterification, the autocatalysis contribution was subtracted out [37]. The catalytic activities

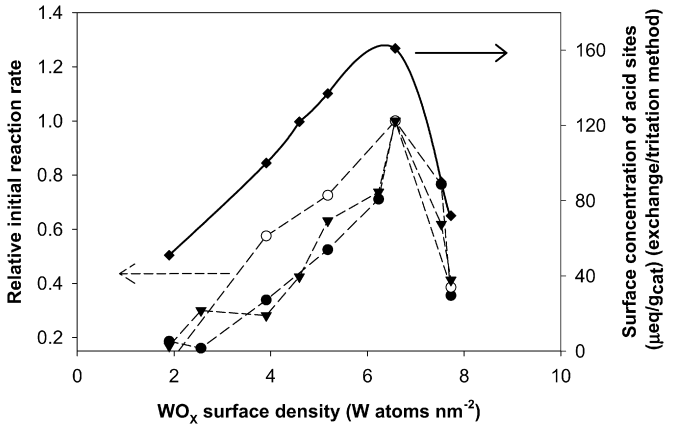

Fig. 5. Relative catalytic activity (with respect to the activity of the catalyst calcined at 800 °C) for the esterification of acetic acid in the gas phase (●), the liquid phase (○), and transesterification of triacetin in the liquid phase (▼). Surface concentration of acid sites determined by exchange-titration method (◆) as a function of the surface concentration of tungsten atoms.

depended significantly on the calcination temperature, and the optimum calcination temperature was found to be 800 °C for all cases. The existence of the same optimum calcination temperature for all reactions indicates the relationship between catalyst physicochemical properties, such as the crystalline structure and molecular structure of the metal oxide overlayer and acid site density and strength. Higher esterification and transesterification rates occurred on samples with near-saturation W surface densities (5–6 W-atoms nm^{-2} [20])—in other words, a catalyst surface on which the W atoms are still largely dispersed. Interestingly, the formation of crystalline WO_3 (at about 800 °C) did not have an immediate detrimental effect on catalyst activity, which is likely attributable to the continued presence of tungsten oxide polymeric structures (as observed by Raman). It was only after a significant disappearance of the heteropolyoxotungstate clusters (to form crystalline WO_3) that the decay in catalytic activity was observed, suggesting that the clusters were the catalytically active sites.

A plot of the relative initial reaction rates (i.e., reaction rates for catalysts calcined at T divided by the reaction rate observed with the catalyst calcined at 800 °C) of esterification and transesterification versus WO_x surface density is shown in Fig. 5. Clearly, the surface concentration of acid sites determined by the ion-exchange/titration method (shown also in Fig. 5) better predicts the catalyst activity than the values obtained by NH_3-TPD method (not plotted). In a related study, a variation of the regular NH_3-TPD methodology using water vapor treatment was also found to give a good prediction of the catalyst activity for skeletal isomerization of n-butane to isobutene on WZ [29].

Ramu et al. [14] reported an optimum calcination temperature of 500 °C for the esterification of palmitic acid using a WZ catalyst containing 5 wt% tungsten. These authors concluded that higher catalytic activity was achieved when the catalyst consisted of a tetragonal phase of ZrO_2 and an X-ray–amorphous form of WO_3. Moreover, they were able to correlate the catalyst activity to the percentage of tetragonal phase. Our results are in qualitative agreement with this observation, in the sense that the formation of what appears to be monoclinic ZrO_2 (as detected using powder XRD and Raman spectroscopy) coincides with the decreased esterification and transesterification rates. However, the optimum calcination temperature reported in this work is approximately 300 °C higher.

Iglesia et al. [20] found that the activity of WZ catalyst (12 wt% W) for the skeletal isomerization of o-xylene to m- and p-xylene passed through a maximum at a calcination temperature of ca. 825 °C. These authors showed that maximum turnover rate for this reaction was achieved at WO_x densities of 10 W-atoms nm^{-2} (greater than theoretical monolayer capacity). The catalytic activity of WO_x species was proposed to be controlled only by the WO_x surface density. Similar results were obtained for 2-butanol dehydration on WZ, with rates reaching a maximum value at WO_x surface densities of ∼8.8 W-atoms nm^{-2} [22]. In the present study, the maximum initial reaction rates results are consistent with these previous findings, in the sense that the growth of polytungstate species at WO_x surface densities slightly higher than a monolayer coverage is required for the development of the maximum number of active sites.

3.3. Brønsted versus Lewis acid sites

Determining the type of acid sites most active for esterification and transesterification is vital. To address this issue, initial transesterification rates were measured on WZ (calcined at 800 °C, WZ800) pre-exposed to different amounts of organic bases. Brønsted acid sites were selectively saturated overnight at 60 °C (with agitation) using a 2,6-di-*tert*-butylpyridine (DTBPy)/methanol solution [41,42] before the reaction. Similarly, a pyridine (Py)/methanol solution was used to poison both Brønsted and Lewis acid sites via protonation and coordination, respectively [22]. The amount of poison adsorbed by the catalyst was determined by taking the difference between the amount of organic base added and that remaining in the liquid adsorption mixture. No organic base desorption was detectable during the course of the transesterification experiment (∼1.5 h), indicating that the organic bases strongly adsorbed on the acid sites of the catalyst.

Fig. 6 shows the relative transesterification rate ($r_{\text{poisoned}}/r_{\text{not poisoned}}$) as a function of adsorbed organic titrant. Interestingly, overlapping of the two curves was observed, indicating that only Brønsted acid sites were active for reaction carried out at 60 °C. This result is not obvious, considering that recent investigations dealing with homogeneous (metal carboxylic salts [43]) and heterogeneous (double-metal cyanide complexes [44]) acid catalysts have reported that Lewis sites can effectively catalyze both esterification and transesterification reactions. In the particular case of supported tungsten oxides, Iglesias et al. [22] showed that the contribution from Lewis acidity may be influenced by the nature of the support (ZrO_2, Al_2O_3, SiO_2, and SnO_2). However, using a calcination temperature of 750 °C, WZ Brønsted acid sites were shown to be solely responsible for catalyzing the dehydration of 2-butanol [23], in good agreement with our present observations.

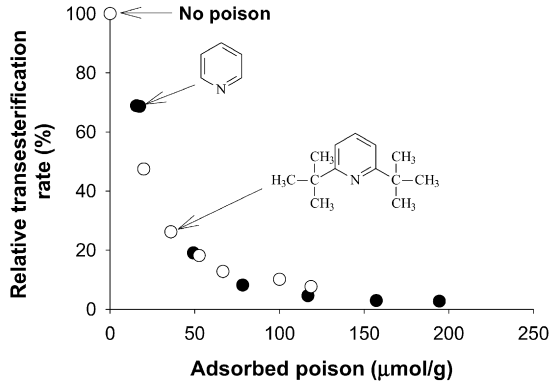

Fig. 6. Relative involvement of WZ800 Brønsted and Lewis acid sites in the transesterification of triacetin with methanol ($T_{rxn} = 60\,^{\circ}C$, $T_{calc} = 800\,^{\circ}C$).

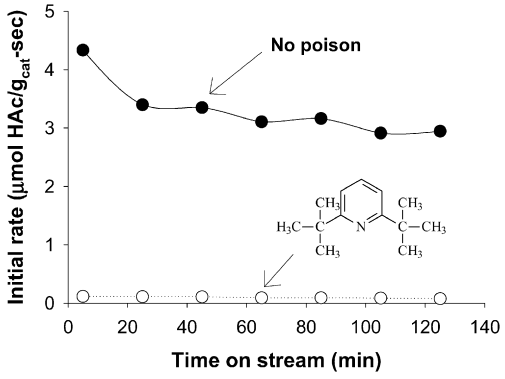

Fig. 7. Comparison of the catalytic activity of WZ800 with no poison and after saturation with DTBPy for the gas-phase esterification of acetic acid with methanol at 120 °C.

To corroborate that these reactions were carried out predominately by Brønsted acid sites on WZ800, selective poisoning of acid sites was also carried out before the gas-phase esterification of acetic acid with methanol. After the in situ dehydration of WZ800 at 315 °C, a flow of DTBPy/He from a saturator was used to poison all Brønsted acid sites (contact time = 2 h [45]) before reaction. Fig. 7 shows that essentially all of the catalyst activity was lost after the catalyst was saturated with DTBPy (that only poisoned Brønsted acid sites). Only a residual activity of ∼3% remained after saturation which is in good agreement with the activity loss observed in the liquid-phase transesterification of triacetin. This result confirms our previous suggestion that Brønsted acidity is primarily responsible for WZ activity for these reactions.

3.4. Genesis of WZ Brønsted acid sites

This section deals with the examination of whether WZ800 Brønsted acid sites originated in situ during reaction or were present after calcination. An IR spectrum was recorded for WZ800 (using Py as the adsorbate) to observe the types of acid sites present in the sample. However, a clear distinction was not possible due to the broadness of the bands (data not shown). Therefore, an equilibrium adsorption experiment was performed in which a 2 ± 0.1 mmol/L solution of DTBPy was used to poison the Brønsted acid sites on WZ800 in the presence of MeOH, THF, or triacetin. In all cases, at least two determinations were made. Table 3 shows that the adsorption of the titrant (i.e., DTBPy) on the solid catalyst took place regardless of the liquid solvent used. The differences in the concentration of adsorbed DTBPy on the catalyst ($C_{DTBPy,\ WZ800}$) may be attributed to variations in the competitive adsorption on the sites (e.g., methanol is a weak base, THF may also exhibit an interaction with Brønsted sites [46]). Although the results are not conclusive as to whether the reactants are able to modify the WZ800 surface, the fact that the catalyst adsorbed a considerable amount of DTBPy in the presence of THF (47 μmol/g) indicates that some Brønsted sites were present even before being exposed to the alcohol or triacetin (because THF would not be expected to cause the formation of Brønsted acidity).

Table 3
Equilibrium adsorption of 2,6-di-*tert*-butylpyridine (DTBPy) on WZ calcined at 800 °C for different solvents at 60 °C

Solvent	Equilibrated concentrations	
	$C_{DTBPy,\ solvent}$ (mmol/L)	$C_{DTBPy,\ WZ800}$ (μmol/g)
Methanol	1.6 ± 0.02	16.0 ± 3.4
THF	1.0 ± 0.02	47.2 ± 2.9
Triacetin	0.5 ± 0.05	76.6 ± 2.7
Methanol + triacetin[a]	0.6 ± 0.04	66.0 ± 2.9

[a] Initial reaction mixture.

Rehydration of Lewis acid sites by sorption of water can occur during cooling of the calcined catalyst [47]. Because in this study, moisture-free air was used during calcination/cooling, with the catalyst then immediately added to the liquid, it is reasonable to suggest that most of the Brønsted acid sites were present after calcination rather than being formed by subsequent adsorption of water. In addition, for the poisoning experiments of gas-phase esterification on WZ800, the catalyst was recalcined at 350 °C just before poisoning and reaction, which also points out the fact that Brønsted sites were present after calcination.

The literature is controversial as to which types of sites are exhibited by WZ calcined at high temperatures. For instance, Brei et al. [25] used transmission IR spectra measurements to show that all Brønsted sites transformed into Lewis acid sites at a calcination temperature of 700 °C or above. For other related solid acids, such as sulfated zirconia, Brønsted acidity is believed to be present only for calcination temperatures below 650 °C [47]. Different viewpoints have been taken by other investigators. For example, Larsen et al. [48] observed that a WZ sample calcined at 800 °C presented DRIFTS bands (at 1640 and 1535 cm^{-1}) corresponding to pyridine adsorbed on Brønsted acid sites. Moreover, Di Gregorio and Keller [30] showed that during WZ calcination, part of the Lewis sites can be converted by condensation into Brønsted acidic sites. Soled et al. [49] found a similar increase in Brønsted acidity for WO_3 on γ-Al_2O_3 with increasing calcination temperature from 500 to 950 °C. Our results also demonstrate the possibility that a large part of the Brønsted sites are present even after calcination at 800 °C.

4. Conclusion

The liquid-phase transesterification of triacetin with methanol at 60 °C and esterification of acetic acid with methanol at 60 °C (liquid phase) and 120 °C (gas phase) were investigated to characterize the effect of calcination temperature on tungstated zirconia catalytic activity. The results showed a strong influence of calcination temperature on the activity for both of these reactions. The most active form of WZ occurred at a surface WO_x density of 6.6 W-atoms nm^{-2}, higher than that required for saturation coverage (5–6 W-atoms nm^{-2}). The increase in esterification and transesterification catalytic activity coincided with the formation of polymeric tungsten species in the presence of the tetragonal phase of the ZrO_2 support. The activity drop at high WO_x surface densities (>6.6 W-atoms nm^{-2}) is attributed to the loss of active sites. Selective poisoning experiments showed that Brønsted acid sites apparently contribute most of the activity. The optimum calcination temperature for WZ was identical for all transesterification and esterification conditions studied. The aqueous exchange-titration method used for estimation of acid site density was better able to predict the catalytic activity than the NH_3-TPD method.

Acknowledgments

This work was supported by the U.S. Department of Agriculture (award 68-3A75-3-147). The authors gratefully acknowledge Magnesium Electron, Inc. (MEI) for providing the WZ precursor. They thank Dr. Donald Van Derveer of Clemson University for his valuable help with the analysis of powder XRD results, and Giriprasath Gururajan and Dan Sweeney at Clemson University for assistance with Raman spectroscopy and TGA analyses, respectively.

References

[1] M. Canakci, J. Van Gerpen, T. ASAE 46 (2003) 945.
[2] M. Canakci, J. Van Gerpen, T. ASAE 42 (1999) 1203.
[3] M. Canakci, J. Van Gerpen, T. ASAE 44 (2001) 1429.
[4] M.J. Goff, N.S. Bauer, S. Lopes, W.R. Sutterlin, G.J. Suppes, J. Am. Oil Chem. Soc. 81 (2004) 415.
[5] S. Zheng, M. Kates, M.A. Dube, D.D. McLean, Biomass Bioenergy 30 (2006) 267.
[6] E. Lotero, Y. Liu, D.E. Lopez, K. Suwannakarn, D.A. Bruce, J.G. Goodwin Jr., Ind. Eng. Chem. Res. 44 (2005) 5353.
[7] D.E. López, J.G. Goodwin Jr., D.A. Bruce, E. Lotero, Appl. Catal. A Gen. 295 (2005) 97.
[8] D.E. López, J.G. Goodwin Jr., D.A. Bruce, J. Catal. 245 (2007) 379.
[9] J. Jitputti, B. Kitiyanan, P. Rangsunvigit, K. Bunyakiat, L. Attanatho, P. Jenvanitpanjakul, Chem. Eng. J. 116 (2006) 61.
[10] Y. Liu, E. Lotero, J.G. Goodwin Jr., J. Catal. 242 (2006) 278.
[11] Y. Liu, E. Lotero, J.G. Goodwin Jr., J. Catal. 243 (2006) 221.
[12] T.A. Nijhuis, A.E.W. Beers, F. Kapteijn, J.A. Moulijn, Chem. Eng. Sci. 57 (2002) 1627.
[13] S. Furuta, H. Matsuhashi, K. Arata, Catal. Commun. 5 (2004) 721.
[14] S. Ramu, N. Lingaiah, B.L.A. Prabhavathi Devi, R.V.N. Prasad, I. Suryanarayana, P.S. Sai Prasad, Appl. Catal. 276 (2004) 163.
[15] K.N. Rao, A. Sridhar, A.F. Lee, S.J. Tavener, N.A. Young, K. Wilson, Green Chem. 8 (2006) 790.
[16] X.R. Chen, C.L. Chen, N.P. Xu, C.Y. Mou, Chin. J. Catal. 24 (2003) 924.
[17] K. Arata, M. Hino, in: Proceedings of the 9th International Congress on Catalysis, 1988, p. 1727.
[18] M. Hino, K. Arata, J. Chem. Soc. Chem. Commun. (1988) 1259.
[19] M. Scheithauer, T.-K. Cheung, R.E. Jentoft, R.K. Grasselli, B.C. Gates, H. Knözinger, J. Catal. 180 (1998) 1.
[20] E. Iglesia, D.G. Barton, S.L. Soled, S. Miseo, J.E. Baumgartner, W.E. Gates, G.A. Fuentes, G.D. Meitzner, Stud. Surf. Sci. Catal. 101 (1996) 533.
[21] L.M. Petrovic, J.R. Bielenberg, G. Larsen, J. Catal. 178 (1998) 533.
[22] J. Macht, C.D. Baertsch, M. May-Lozano, S.L. Soled, Y. Wang, E. Iglesia, J. Catal. 227 (2004) 479.
[23] C.D. Baertsch, K.T. Komala, Y.-H. Chua, E. Iglesia, J. Catal. 205 (2002) 44.
[24] E. Torres-García, G. Rosas, J.A. Ascencio, E. Haro-Poniatwski, R. Pérez, Appl. Phys. A 79 (2004) 401.
[25] V.V. Brei, O.V. Melezhyk, S.V. Prudius, G.M. Tel'biz, O.I. Oranska, Adsorp. Sci. Tech. 23 (2005) 109.
[26] K. Shimizu, T.N. Venkatraman, W. Song, Appl. Catal. A Gen. 225 (2002) 33.
[27] T. Onfroy, G. Clet, M. Houalla, Chem. Commun. (2001) 1378.
[28] M. Valigi, D. Gazzoli, I. Pettiti, G. Mattei, S. Colonna, S. De Rossi, G. Ferraris, Appl. Catal. A Gen. 231 (2002) 159.
[29] N. Naito, N. Katada, M. Niwa, J. Phys. Chem. B 103 (1999) 7206.
[30] F. Di Gregorio, V. Keller, J. Catal. 225 (2004) 45.
[31] D.G. Barton, M. Shtein, R.D. Wilson, S.L. Soled, E. Iglesia, J. Phys. Chem. B 103 (1999) 630.
[32] N. Vaidyanathan, D.M. Hercules, M. Houalla, Anal. Bioanal. Chem. 373 (2002) 547.
[33] D.G. Barton, S.L. Soled, G.D. Meitzner, G.A. Fuentes, E. Iglesia, J. Catal. 81 (1999) 57.
[34] J.G. Santiesteban, J.C. Vartuli, S. Han, R.D. Bastian, C.D. Chang, J. Catal. 168 (1997) 431.
[35] R.A. Boyse, E.I. Ko, Appl. Catal. A Gen. 177 (1999) L131.
[36] D.G. Barton, S.L. Soled, E. Iglesia, Top. Catal. 6 (1998) 87.
[37] Y. Liu, E. Lotero, J.G. Goodwin Jr., J. Mol. Catal. A Chem. 245 (2005) 132.
[38] M. Kilo, C. Schild, A. Wokaun, J. Chem. Soc. Faraday Trans. 88 (1992) 1453.
[39] S. Kuba, P.C. Hedorn, R.K. Grasselli, B.C. Gates, M. Che, H. Knözinger, Phys. Chem. Chem. Phys. 3 (2001) 146.
[40] I.E. Wachs, T. Kim, E.I. Ross, Catal. Today 116 (2006) 162.
[41] H.C. Brown, R.B. Johanneson, J. Am. Chem. Soc. 75 (1953) 16.
[42] A. Corma, V. Fornés, L. Forni, F. Máquez, J. Martínez-Triguero, D. Moscotti, J. Catal. 179 (1998) 451.
[43] M. Di Sergio, R. Tesser, M. Dimiccoli, F. Cammarota, M. Nastasi, E. Santacesaria, J. Mol. Catal. A Chem. 239 (2005) 111.
[44] P.S. Sreeprasanth, R. Srivastava, D. Srinivas, P. Ratmasamy, Appl. Catal. A Gen. 314 (2006) 148.
[45] K. Suwannakarn, E. Lotero, J.G. Goodwin Jr., in press.
[46] C. Pazé, C. Bordiga, C. Lamberti, M. Salvalaggio, A. Zecchina, J. Phys. Chem. B 101 (1997) 4740.
[47] A. Clearfield, G.P.D. Serrete, A. Khazisyed, Catal. Today 20 (1994) 295.
[48] G. Larsen, S. Raghavan, M. Marquéz, E. Lotero, Catal. Lett. 37 (1995) 57.
[49] S.L. Soled, G.B. McVicker, L.L. Murrel, L.G. Sherman, N.C. Dispenziere, S.L. Hsu, D. Waldman, J. Catal. 111 (1988) 286.
[50] S.D. Kim, M. Ostromecki, I.E. Wachs, J. Mol. Catal. A Chem. 106 (1996) 93.
[51] M. Scheithauer, R.K. Grasselli, H. Knözinger, Langmuir 14 (1998) 3019.